I Introduction to basic radiometry concepts

Radiometry is the field of science devoted to the measurement of the thermal electromagnetic energy radiated by the bodies. Since the appearance of man-made satellites, radiometry has played an important role in remote sensing. The measurement of the small electromagnetic energy emitted by the outer space concerns to radio-astronomy. A radiometer is an instrument that measures the brightness, that is, the power emitted by a body by unit solid angle, and by unit surface, with high resolution and accuracy.

I.1 Brightness and power collected by an antenna

The power emitted by a body in a solid angle by unit surface is called the brightness, units [W sr^{-1} m^{-2}]. If the emitting surface radiates with a pattern $F_t(\theta,\phi)$, the brightness $B(\theta,\phi)$ is given by:

$$B(\theta,\phi)=\frac{F_t(\theta,\phi)}{A_t}, \tag{1.1}$$

where A_t is the total area which is radiating.

The power collected by an antenna surrounded by a distribution of incident power $B(\theta,\phi)$ can be computed as [1],

$$P=F_t\cdot\frac{A_r}{R^2}=B\cdot A_t\cdot\frac{A_r}{R^2}, \tag{1.2}$$

being A_r the effective area of the antenna and R the distance to the radiating surface.

Taking into account that the solid angle Ω_t subtended by the transmitting antenna is defined by:

$$\Omega_t=\frac{A_t}{R^2}, \tag{1.3}$$

then, the power collected by the antenna can be computed as:

$$P = B\cdot A_r\cdot\Omega_t. \tag{1.4}$$

Replacing the solid angle by a differential solid angle ($d\Omega$), the corresponding power received by the antenna from an extended source of incidence brightness $B(\theta,\phi)$ can be expressed (Figure 1.1) as:

$$dP=A_r\cdot B(\theta,\phi)\cdot\left|F_n(\theta,\phi)\right|^2, \tag{1.5}$$

where $|F_n(\theta,\phi)|^2$ is the normalized antenna radiation pattern. Moreover, if the brightness is not constant with frequency, a new magnitude must be defined: the spectral brightness density $B_f(\theta,\phi)$, units [W sr^{-1} m^{-2}

Hz^{-1}]. The total power collected by the antenna is then obtained by integrating expression (1.5) over the system's bandwidth and over the space:

$$P = \frac{1}{2} \cdot A_r \int_{f}^{f+B} \iint_{4\pi} B_f(\theta,\phi) \cdot |F_n(\theta,\phi)|^2 \cdot d\Omega \cdot df \tag{1.6}$$

where B is the bandwidth of the receiving system. Since the antenna collects only half of the randomly polarized thermal power emitted, it is multiplied by a factor $1/2$.

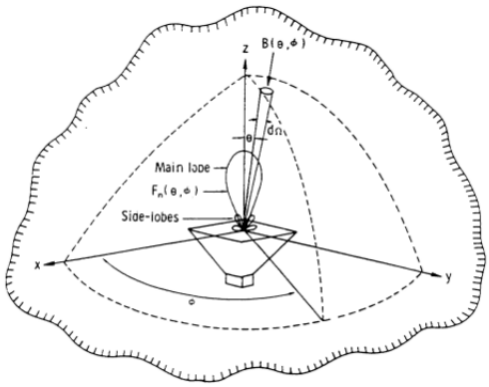

Figure 1.1. Geometry of the radiation incident over the antenna [1, p.189].

I.2 Thermal radiation

I.2.1 Quantum Theory of Radiation

All bodies at a finite absolute temperature radiate electromagnetic energy. According to Bohr's equation, the frequency f of an emitted radiation is given by:

$$f = \frac{\varepsilon_1 - \varepsilon_2}{h}, \tag{1.7}$$

where:

ε_1 and ε_2 are different energy levels [J],

h is the Planck's constant ($h = 6.63 \cdot 10^{-34}$ J).

The emission of radiation is caused by the collision between the particles. The collision probability is a function of the density of the particles and the kinetic energy of their random motion. The increase of the intensity of the energy radiated by a body is proportional to the increase of its absolute temperature.

I.2.2 Planck's black-body radiation's law

In general, part of the electromagnetic energy incident on a surface is absorbed, and part is reflected. The spectral brightness (brightness per unit bandwidth) is given by the Planck's law (1.8).

$$B_f = \frac{2 \cdot h \cdot f^3}{c^2} \cdot \frac{1}{e^{h\,f/kT_o} - 1}, \tag{1.8}$$

where:

f is the frequency in Hertz,

k is the Boltzmann's constant ($k = 1.38 \cdot 10^{-23}$ J K^{-1}),

T_o is the absolute physical temperature in Kelvin, and

c is the speed of light ($c = 3 \cdot 10^8$ m s^{-1}).

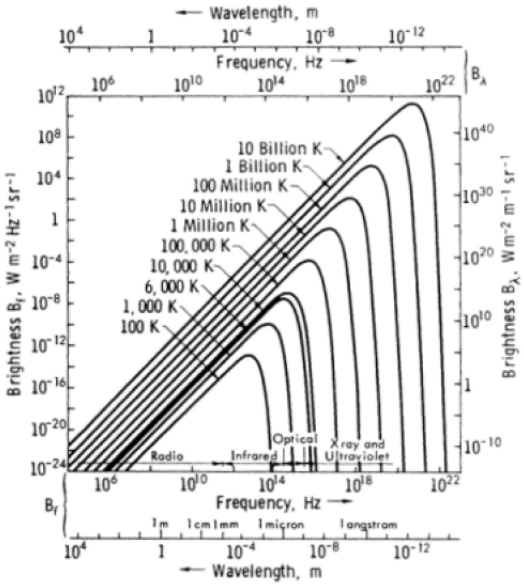

Figure 1.2. Planck's radiation law [1, p. 193].

Applying the Taylor's approximation to the exponential function in eqn. (1.8), the exponent $h\,f\,/\,k\,T_o$ in the denominator of Planck's law is far smaller than 1 at microwave frequencies, and therefore, the following approximation can be used to simplify eqn. (1.8).

$$e^x - 1 = 1 + x + \frac{x^2}{2} + \ldots - 1 \approx x \;\; for \;\; x << 1. \tag{1.9}$$

Hence, at low microwave frequencies the Rayleigh-Jeans law can be used as good approximation of the Planck's law (1.8) and can be written as:

$$B_f = \frac{2 \cdot f^2 \cdot k \cdot T_{phys}}{c^2} = \frac{2 \cdot k \cdot T_{phys}}{\lambda^2}. \tag{1.10}$$

In this case, if λ and T_o appearing eqn. (1.10) satisfy that:

$$\lambda \cdot T_o > 0.77\, m\, K, \;\; \frac{f}{T_o} < 3.9 \cdot 10^8\, Hz \cdot K^{-1}, \tag{1.11}$$

the error committed by the Rayleigh-Jeans' approximation is smaller than 1%, if the physical temperature is 300 K and the frequency is smaller than 117 GHz, which covers a large part of the microwave spectrum. Expression (1.10) will be used from now on. Note that there is a linear relation between the spectral brightness density and the physical temperature.

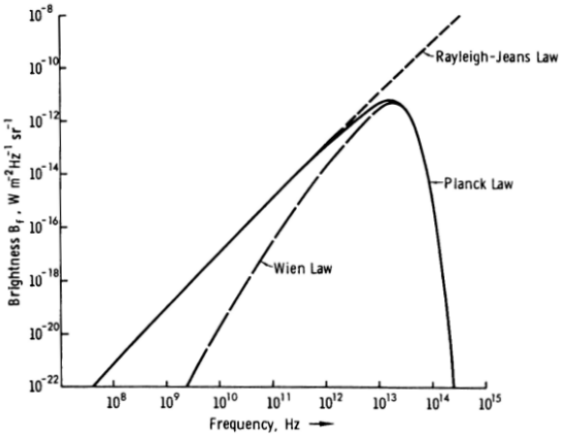

Figure 1.3. Comparison of Planck's law with its low-frequency (Rayleigh-Jeans law) and high-frequency (Wien's law) approximations at 300 K [1, p.198].

I.2.3 Power-temperature correspondence

The power received by an antenna with normalized radiation pattern $|F_n(\theta,\phi)|^2$, placed inside of a black-body chamber at a constant physical temperature T_o is (Figure 1.4)

$$P_{bb} = \frac{1}{2} \cdot A_r \cdot \int_{f}^{f+B} \iint_{4\pi} \frac{2 \cdot k \cdot T_o}{\lambda^2} |F_n(\theta,\phi)|^2 \, d\Omega \cdot df, \tag{1.12}$$

where the subscript *bb* stands for black-body.

The detected power will be limited by the antenna bandwidth *B*. If this bandwidth is small enough to assume that the spectral brightness density does not change over the frequency range, eqn. (1.12) reduces to:

$$P_{bb} = k \cdot T_o \cdot B \cdot \frac{A_r}{\lambda^2} \cdot \iint_{4\pi} |F_n(\theta,\phi)|^2 \, d\Omega = k \cdot T_o \cdot B, \tag{1.13}$$

where the antenna solid angle has been expressed as a function of its effective area:

$$\Omega_p = \iint_{4\pi} |F_n(\theta,\phi)|^2 \, d\Omega = \frac{\lambda^2}{A_r}. \tag{1.14}$$

Eqn. (1.13) shows a linear relationship between the physical temperature of a body and the power collected by an antenna. In 1928, Nyquist found the same expression (eqn. (1.15)) for the available power

at the terminals of a resistance at a physical temperature T_o. This means that, for an ideal receiver of bandwidth B, the antenna delivers to the load the same power as a resistance at a temperature T_A, which is called the antenna temperature:

$$P = k \cdot T_o \cdot B. \tag{1.15}$$

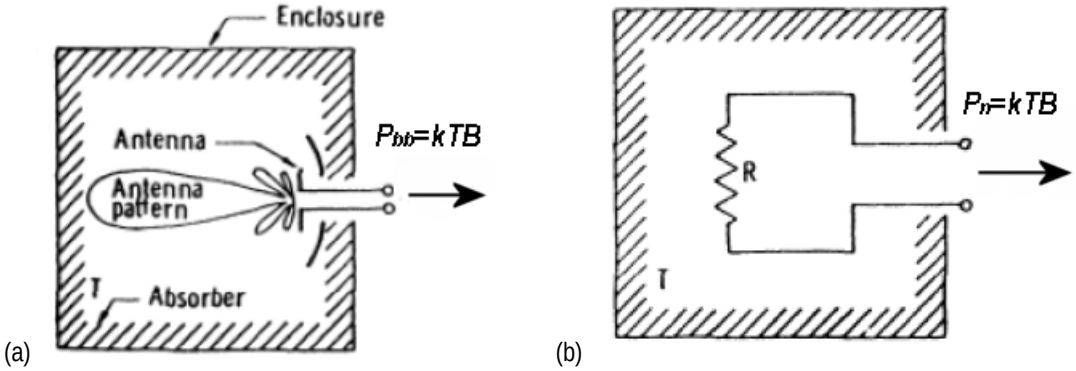

Figure 1.4. The power delivered by: (a) an antenna placed inside of a black-body enclosure of temperature T is equal to the power delivered by (b) a resistor maintained at the same physical T (assuming each one is connected to a matched receiver of bandwidth B [1, p. 199].

I.2.4 Gray-body radiation

I.2.4.1 Brightness temperature and emissivity

A black-body is an idealized body and it is a perfect emitter. These bodies absorb all the incidence energy, and when the thermodynamic equilibrium is reached at physical temperature T_o , they radiate all the energy omni-directionally. However, real materials (usually called gray-bodies) emit less energy than a black-body since they do not absorb all the energy incident on them. Since the universe is composed of gray-bodies two new concepts are introduced, the brightness temperature $(T_B(\theta,\phi))$ and the emissivity $(e(\theta,\phi))$. Equation (1.16) shows, the relationship between these two concepts

$$e(\theta,\phi) = \frac{B(\theta,\phi)}{B_{bb}} = \frac{T_B(\theta,\phi)}{T_o}, \tag{1.16}$$

where B_{bb} is the brightness of the black-body at a temperature T_o.

The brightness temperature emitted by a black-body coincides with its physical temperature hence its emissivity is 1. Consequently the brightness temperature emitted by real bodies is less than their physical temperature, and then their range of emissivity values are between 0 and 1. In conclusion, the emissivity of a perfect reflecting material is equal to zero and the emissivity of a perfect absorber is one.

I.2.4.2 The apparent temperature

The apparent temperature (T_{AP}) is an equivalent temperature related to the total brightness incident over the antenna, $B_i(\theta,\phi)$:

$$B_i(\theta,\phi)=\frac{2\cdot k}{\lambda^2}\cdot T_{AP}(\theta,\phi)\cdot B \tag{1.17}$$

In remote sensing applications, the T_B of the surface is measured by an antenna far away (Figure 1.5). In this case, the apparent temperature T_{AP} is the key parameter that depends on:

- the brightness temperature of the surface under observation (T_B),
- the atmospheric upward radiation (T_{UP}),
- the atmospheric downward radiation scattered reflected by the surface (T_{SC}), and
- the atmospheric attenuation (L_a),

and can be written as:

$$T_{AP}=T_{UP}+\frac{1}{L_a}\cdot(T_B+T_{SC}). \tag{1.18}$$

By observing eqn. (1.18), when the atmospheric losses are high, the apparent temperature is almost equal to the atmospheric temperature. It happens at high frequencies or at the absorption windows of some gases. It is important to take into account the atmospheric attenuation if the brightness temperature of the Earth is measured. In the frequency range from 1 GHz to 10 GHz losses for a cloud-free atmosphere are very small and can be neglected. Consequently the apparent brightness temperature (T_{AP}) can be approximated by the brightness temperature (T_B).

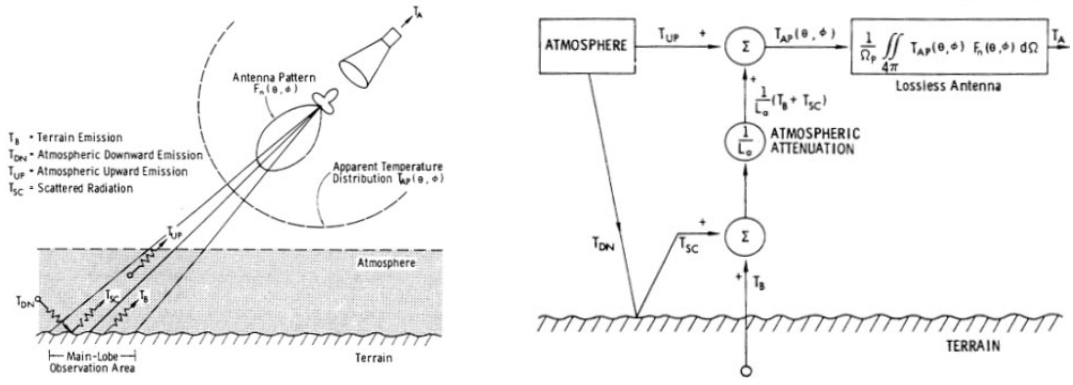

Figure 1.5. Relationship between the antenna temperature T_A, the apparent temperature T_{AP} and the brightness temperature T_B [1, p. 202].

According to Figure 1.5 and taken into account the normalized antenna pattern $(F_n(\theta,\phi))$ and the normalized by the pattern solid angle (Ω_p), the antenna temperature is given by:

$$T_A = \frac{1}{\Omega_p} \iint_{4\pi} T_{AP}(\theta,\phi)\,|F_n(\theta,\phi)|^2\, d\Omega \tag{1.19}$$

I.3 Perturbations in the measurement of the brightness temperature

The brightness temperature measurements taken from the space are perturbed by some phenomena as the Faraday rotation, the space radiation and the atmospheric effects, that are necessary to take into account and sometimes they cannot be avoided.

I.3.1 Faraday rotation

Faraday rotation is based on the rotation of the plane of polarization of the electromagnetic waves propagating through the ionosphere. According to [2, p. 121], the mean rotation value can be estimated as:

$$\varphi \approx \frac{17^{\circ}}{f^2_{[GHz]}}\,. \tag{1.20}$$

At low frequencies this effect cannot be neglected. At L-band (1.4 GHz) the average rotation is found at φ = 8.7°.

I.3.2 Space radiation

The apparent temperature is modified by the contribution of the microwave radiation emitted from the space. Three main phenomena can be considered, and their contribution to the antenna temperature needs to take into account the averaging by the antenna pattern.

- Cosmic radiation level is fairly constant, about 2.7 K, and does not affect the quality of the measurement,
- Galactic noise at L-band presents large variations, from 0.8 K to 40 K depending if the pole or the center of the galaxy is reflected over the Earth's surface. The correction is feasible because the galactic noise is well mapped, although the absolutely accuracy of these maps is still an open issue.
- Sun glints can affect the measurements because the Sun brightness temperature value is higher than 100,000 K. Hence, direct reflections can be avoided by pointing the instrument to the dark zone of a polar sun-synchronous orbit.

I.4 Framework and organization of this Ph.D.thesis

The improvement of weather predictions, e.g. for natural catastrophes, requires the knowledge of Soil Moisture (*SM*) and Sea Surface Salinity (*SSS*) at a global scale. Nowadays, the amount of water over land, the energy exchange between the land surface and the atmosphere, the evaporation and the infiltration can be traced through the *SM*. Hence, the temporal evolution of this parameter will contribute to improve weather predictions, hydrological studies, vegetation monitoring, and forest fires risk evaluation. At the same time, the knowledge of the ocean salinity distribution at a global scale with a moderate revisit time is important to climate predictions as well, since it is a tracer of sea surface currents, and it is an indicator of the difference between evaporation and precipitation. Water density is determined by salinity, and hence the thermo-haline circulation can also be monitored by SSS measurements. Salinity monitoring will be useful to improve the quality of the ENSO (El Niño Southern Oscillation) numerical model predictions, as well.

In May 1999, the European Space Agency (ESA) selected SMOS (Soil Moisture and Ocean Salinity) as the second Earth Explorer Opportunity mission within the Living Planet Programme, with a launch date in February 2007. One of its goals is the generation of global sea surface salinity maps (e.g. Figure 1.6a). Two dimensional brightness temperature maps will be achieved with a 30 km x 30 km pixel size. To observe salinity variations around 0.1 psu (practical salinity unit) at global scale, it will be necessary perform temporal and spatial averaging (30 days and 200 km respectively). These data products will be applied to improve the climate models and to predict the heat exchanges between the sea, air and land. The sensor aboard SMOS is an L-band dual-polarization radiometer with full-polarimetric capability called MIRAS (*M*icrowave *I*maging *R*adiometer by *A*perture *S*ynthesis, Figure 1.6b).

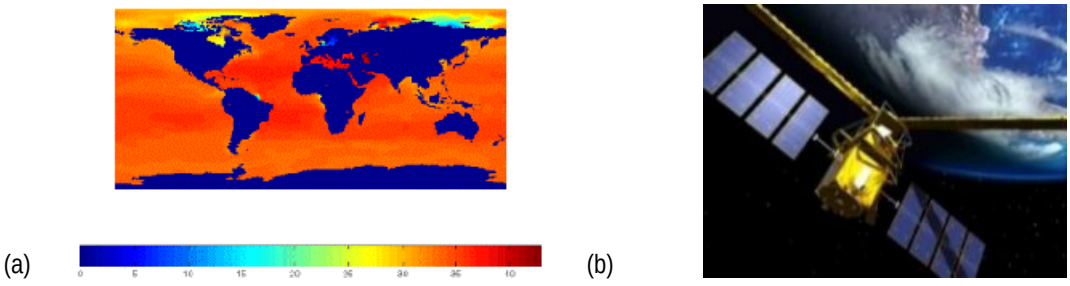

(a) (b)

Figure 1.6. (a) *SSS* Levitus '94 map, and (b) SMOS artist's view.

The retrieval of sea surface salinity (*SSS*) from microwave radiometric measurements is based on the fact that the dielectric constant of seawater is a function of salinity and temperature (Figure 1.7). The sensitivity of the brightness temperature (T_B) to *SSS* at low microwave frequencies is maximum, and the optimum conditions for salinity retrieval are found at L-band, where there is a protected band for passive observations (1.4-1.427 GHz).

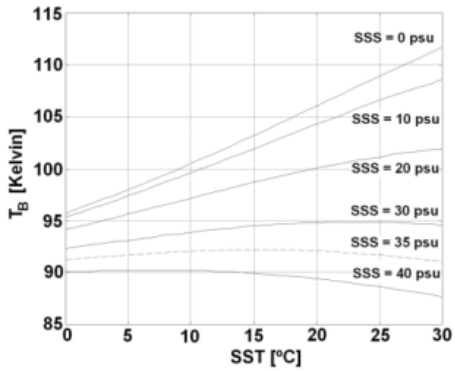

Figure 1.7. Nadir brightness temperature dependence with SSS and SST at 1.4 GHz.

However, even at this frequency the sensitivity of T_B to *SSS* is low: 0.5 K per psu for a sea surface temperature (*SST*) of 20°C, decreasing to 0.25 K per psu for an *SST* of 0°C. Since other variables influence the T_B signal (polarization, incidence angle, sea surface temperature, roughness and foam), unless they are properly accounted for, the *SSS* determination will be erroneous.

(a)

(b)

(c)

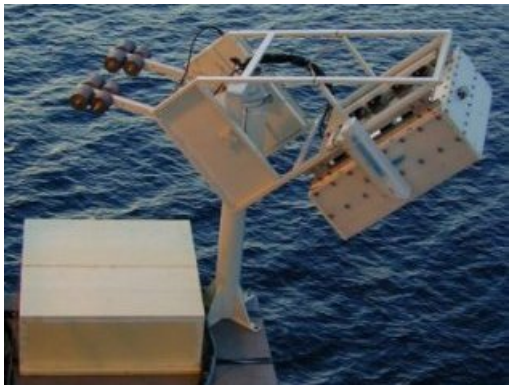

(d)

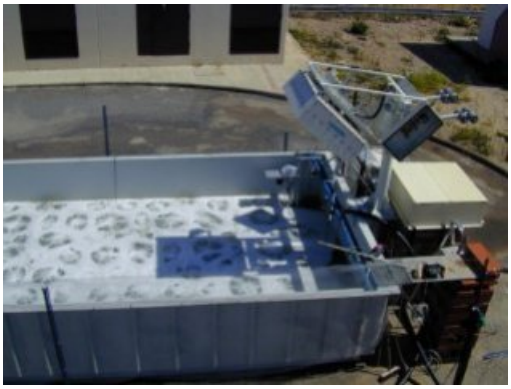

Figure 1.8. (a) Location of the Casablanca oil rig and IRTA facilities, (b) Casablanca oil rig (WISE), (c) radiometric measurements (LAURA), and foam generation (FROG), and (d) rain generation (FROG).

Two field experiments named WISE (WInd and Salinity Experiment) were sponsored by ESA to better understand the wind and sea state effects on the L-band brightness temperatures. They consisted of the acquisition of long time series of T_B to try to relate it to the wind speed (that contributes to the sea surface roughness), significant wave height (*SWH*), and the instantaneous foam coverage. They took place at the Casablanca oil rig (Figure 1.8a to Figure 1.8c), located in the Northern Mediterranean Sea, 40

km off shore the Ebro river delta. WISE 2000 took place from November 25th to December 18th, 2000, and continued during January 9th to 16th, 2001, and WISE 2001 from October 23rd to November 22nd, 2001. Under Spanish National funds, a third field experiment named FROG (Foam, Rain, *O*il slicks and GPS reflectometry, Figure 1.8a and Figure 1.8d) took place from March 23rd to May 5th 2003, at the IRTA (Institut de Recerca i Tecnologia Agroalimentàries) facilities at the Ebro river delta, to measure some effects that were not completely understood during the WISE field experiments: the foam emissivity, and the impact of rain, and oil slicks on the T_B variations. In conclusion, the purpose of these field experiments has been the improvement of the sea surface emissivity models that until now have not clearly included these effects. In order to achieve the objectives of the WISE and FROG field experiments the LAURA L-band full-polarimetric radiometer of the Technical University of Catalonia (UPC) was designed and implemented for these specific field experiments.

In chapter II a detailed description of the LAURA radiometer is made. First of all, a general brief explanation of the types of radiometers is given. The radiometer antenna, the receiver circuitry, and the data acquisition system are explained. Chapters three and four present the WISE 2000 and 2001 experiment plans, the field experiments, the data processing, the experimental results, and the inter-comparison with the theoretical model. The FROG experiment field is explained in chapters five and six.